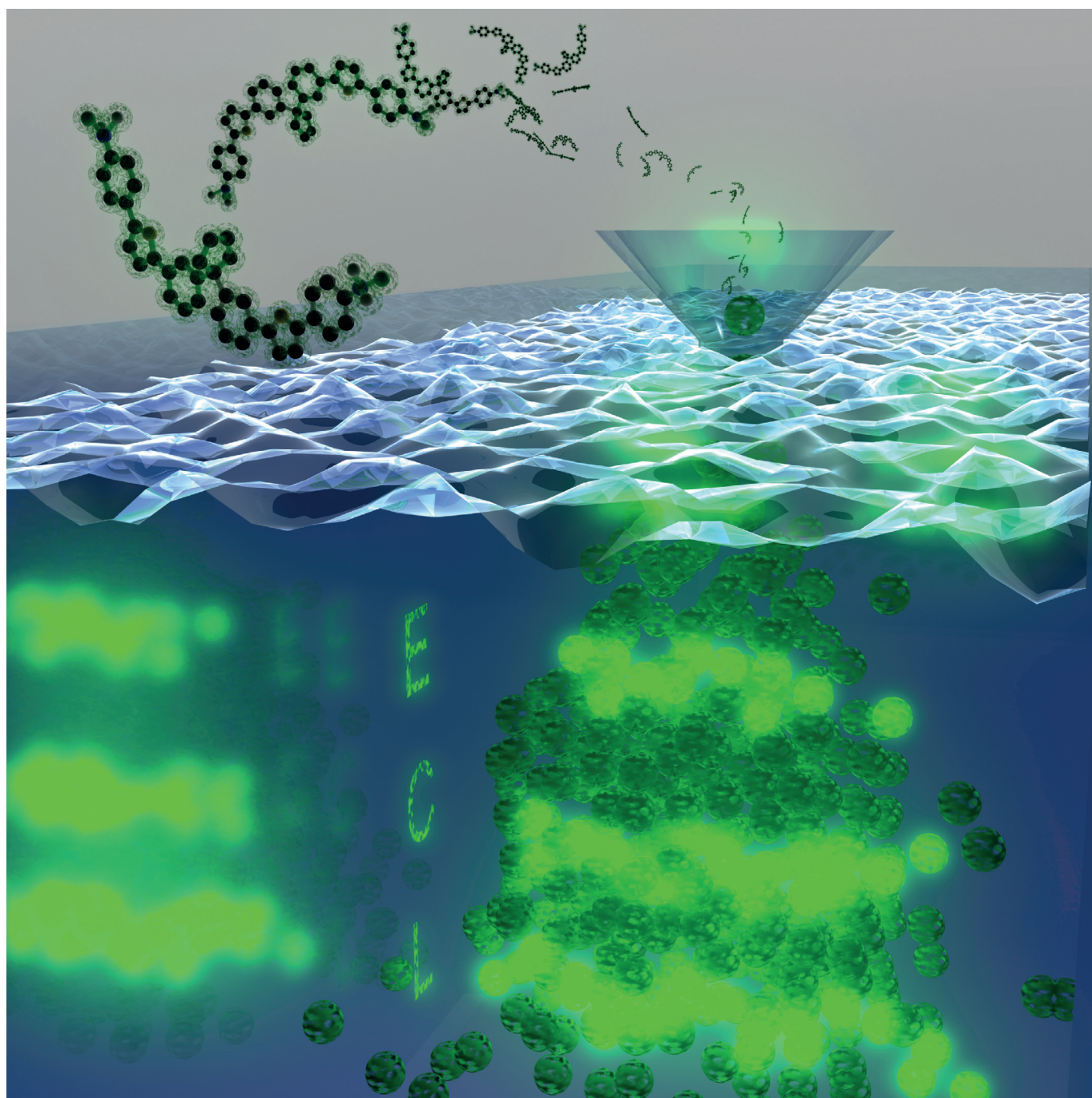


■ Electrogenenerated Chemiluminescence | *Hot Paper* |● **Bright Electrogenenerated Chemiluminescence of a Bis-Donor  
Quadrupolar Spirofluorene Dye and Its Nanoparticles**Haidong Li, Jonathan Daniel, Jean-Baptiste Verlhac, Mireille Blanchard-Desce,\* and  
Neso Sojic\*<sup>[a]</sup>

**Abstract:** A series of symmetric fluorescent dyes built from a spirofluorene core bearing electroactive end groups and having different conjugated linkers were prepared with a view to their use as building blocks for the preparation of electrochemiluminescent (ECL) dyes and nanoparticles. Their electrochemical, spectroelectrochemical, and ECL properties were first investigated in solution, and structure/activity relationships were derived. The electrochemical and ECL properties show drastic variation that could be tuned by means of the nature of the  $\pi$ -conjugated system, the end groups, and the core. In this series, highly fluorescent dye **1** based on a spirofluorene core and triphenylamine end groups connected via thiophene moieties shows the most promising

and intriguing properties. Dye **1** is reversibly oxidized in three well-separated steps and generates a very intense and large ECL signal. Its ECL efficiency is 4.5 times higher than that of the reference compound  $[\text{Ru}(\text{bpy})_3]^{2+}$  (bpy = 2,2'-bipyridine). This remarkably high efficiency is due to the very good stability of the higher oxidized states and it makes **1** a very bright organic ECL luminophore. In addition, thanks to its molecular structure, this dye retains fluorescence after nanoprecipitation in water, which leads to fluorescent organic nanoparticles (FONs). The redox behavior of these FONs shows oxidation waves consistent with the initial molecular species. Finally, ECL from FONs made of **1** was recorded in water and strong ECL nanoemitters are thus obtained.

## Introduction

Materials based on thiophenes and their functional derivatives have been widely investigated in the fields of electroluminescent devices,<sup>[1]</sup> chemosensors,<sup>[2]</sup> and biosensors.<sup>[3]</sup> In particular, oligo/polythiophenes have become the most frequently investigated structures.<sup>[4]</sup> Studies on thiophene have been developed for a long time and are well established.<sup>[5]</sup> Thiophenes are ideal platforms for transition metal catalyzed cross-coupling reactions, which have provided numerous methods for the synthesis of most functionalized thiophene derivatives in the past decades.<sup>[6]</sup> Thiophene-based materials have many outstanding chemical and physical properties, such as their unique variety of electronic properties and easy structural variation.<sup>[7]</sup> Recently, *N*-perarylated aromatic amines have received intense interest due to their use in organic synthesis and structure studies.<sup>[8]</sup> Thiophene derivatives functionalized with *N*-perarylated aromatic amino groups can be used in hole-transporting materials for optical and microelectronic devices, such as organic light-emitting diodes,<sup>[9]</sup> organic field-effect transistors,<sup>[10]</sup> solar cells,<sup>[11]</sup> and photocopiers.<sup>[12]</sup> Many thiophene derivatives with *N*-perarylated aromatic amino moieties have been prepared to investigate the interaction between the two components.<sup>[4c,13]</sup>

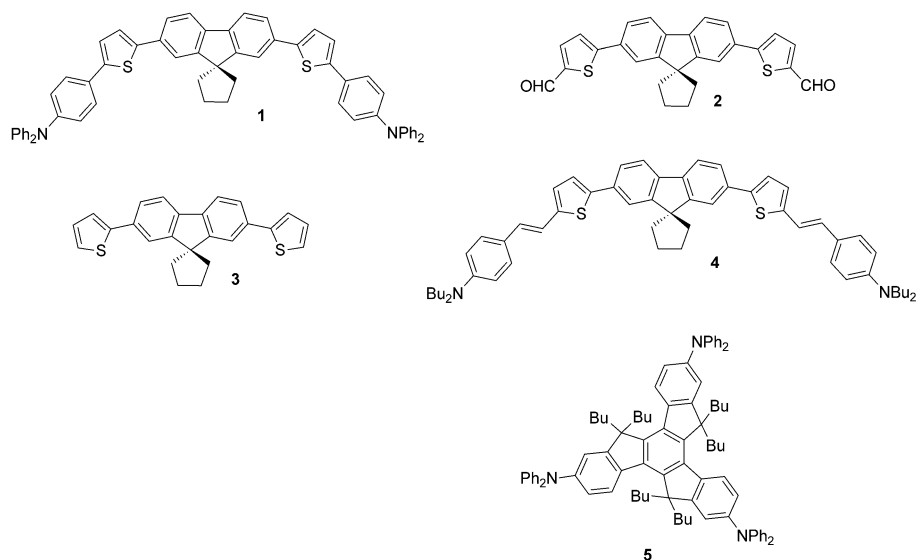
Electrogenerated chemiluminescence (ECL) involves the *in situ* generation of an excited state at an electrode surface by electron-transfer reactions.<sup>[14]</sup> ECL mechanisms follow two dominant pathways. In the annihilation pathway, an oxidized and a reduced species of the luminophore are electrochemically produced at the electrode surface by applying an alternating pulsed potential. Then, these two species diffuse and undergo an annihilation reaction to generate an electronically excited

state, which relaxes to the ground state and emits a photon.<sup>[15]</sup> An alternative mode with more complex kinetic pathways is based on the use of sacrificial coreactants (e.g., tri-*n*-propylamine,<sup>[16]</sup> oxalate,<sup>[17]</sup> benzoyl peroxide)<sup>[18]</sup> capable of reacting with the oxidized or reduced luminophore to generate the desired excited state, which makes ECL very useful in practical applications. Since by essence ECL does not require any external light source for excitation, it is a very sensitive technique that is based on orthogonal electrochemical addressing and optical detection. Due to its interdisciplinary nature and also to its remarkable characteristics, ECL has attracted major interest in different fields such as photochemistry, electrochemistry, and analytical chemistry.<sup>[19]</sup> ECL has shown great achievements not only in fundamental research, but also for real applications, mainly in immunoassays for the diagnostics market.<sup>[20]</sup> The model systems are mainly based on organic dyes such as aromatic heterocycles and organometallic compounds such as tris-cyclometalated ruthenium and iridium complexes.<sup>[21]</sup> To increase the sensitivity and analytical performance of ECL, many efforts are currently focused on the development of novel luminophores and ECL nanoemitters with tunable wavelengths.<sup>[13a,21a,22]</sup> For example, in a remarkable example of self-enhanced ECL based on an iridium-based complex reported by Ding and co-workers, the ECL efficiency increases after each oxidation step.<sup>[22]</sup> Kim et al. described enhanced ECL of pyrene derivatives attributed to the stability of the cation and anion radicals due to peripheral multidonors.<sup>[22n]</sup> In the present work, we exploit a conceptually similar strategy with spirofluorene-based compounds in which the higher oxidized states are stabilized and thus lead to a very intense and large ECL signal.

Recently, the design and synthesis of quadrupolar fluorescent dye **1** (Scheme 1) for the preparation of ultrabright FONs was published by Blanchard-Desce et al.<sup>[23]</sup> This dye is a push–push system based on a spirofluorene core and terminated by triphenylamine moieties as electron-donating end groups. This dye shows interesting properties, including strong absorption in the violet-blue visible region, intense blue-green emission in solution, and the ability to retain fluorescence after aggregation, which leads to fluorescent organic nanoparticles (FONs) with high brightness and good photostability. Moreover, when

[a] H. Li, Dr. J. Daniel, Prof. J.-B. Verlhac, Dr. M. Blanchard-Desce, Prof. N. Sojic  
Université Bordeaux  
ISM, UMR 5255 CNRS  
33400 Talence (France)  
E-mail: mireille.blanchard-desce@u-bordeaux.fr  
neso.sojic@u-bordeaux.fr

Supporting information for this article is available on the WWW under  
<http://dx.doi.org/10.1002/chem.201600413>.



**Scheme 1.** Chemical structures of dyes 1–5.

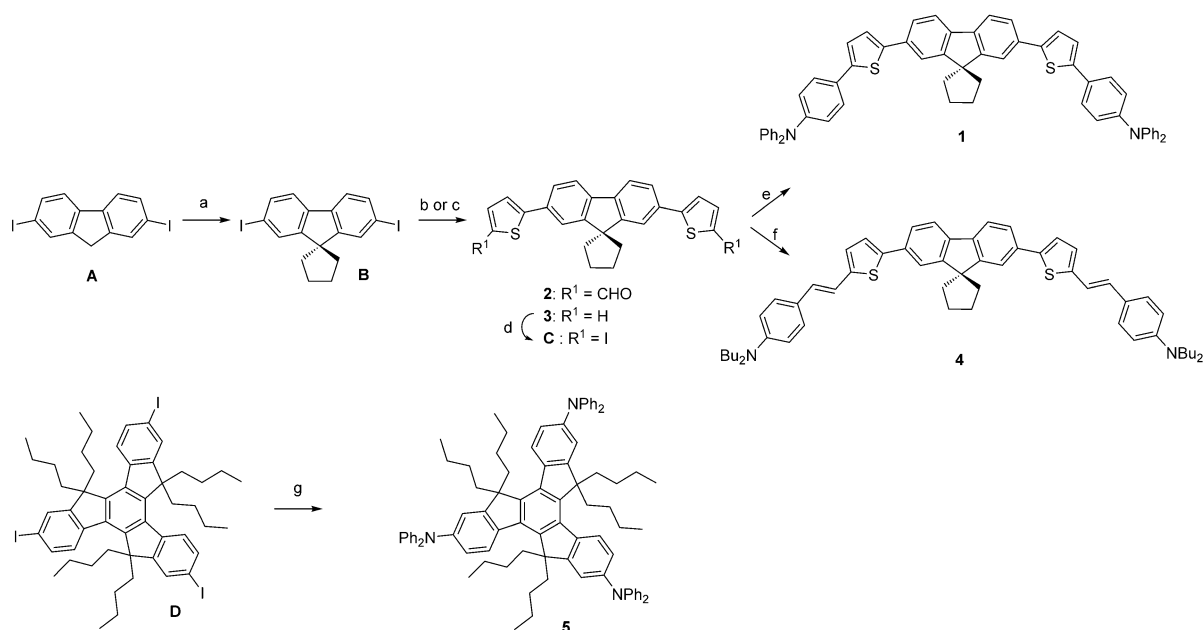
the dye aggregates into nanoparticles in water, its photophysical properties are strongly affected by the molecular confinement. A hypochromic and hypsochromic shift as well as a broadening of the low-energy absorption band is observed, which reveals excitonic coupling between dye subunits in the FONs. A bathochromic shift of the fluorescence emission spectrum is also observed due to excitonic splitting. Compared to dye **1** dissolved in organic solutions, FONs made from dye **1** show somewhat reduced fluorescence quantum yield (from about 0.7 in organic solutions to 0.15 for FONs in water), which is due to both the decrease in the radiative rate (in relation to the redshifted emission and excitonic coupling) and major increase in the nonradiative decay rate (most probably due to efficient vibrational deactivation processes favored by water molecules H-bonded to the nanoparticle surfaces or electron-transfer reactions). Yet, due to the molecular confinement, high brightness is obtained (typically  $2.2 \times 10^8 \text{ M}^{-1} \text{ cm}^{-1}$  for FONs having a radius of about 22 nm), which makes these FONs, of major interest for bioimaging purposes.<sup>[23]</sup> Due to the presence of their electron-donating end groups, we thus posited that such dyes could also generate interesting ECL properties both as individual dyes and FONs. Along this line of thinking, it has already been reported that diarylamino derivatives are able to give stable oxidized species with good ECL capability in organic solvents.<sup>[24]</sup> Even if the fluorene core is a good fluorescence emitting center, the poor stability of the oxidized cation radical makes it an inefficient ECL luminophore. However, its stability can be improved by modifying it with appropriate redox groups such as thiophene.<sup>[25]</sup> The choice of suitable  $\pi$  spacers and terminal groups is crucial, since they can directly influence the energies of the HOMO and LUMO, the absorption spectrum, and the charge separation on photoexcitation. For these reasons, we investigated the electrochemical properties of dye **1** in organic solution and as FONs in buffered water. For comparative studies, and to gain deeper insight into the origin of these luminescence processes and the role of the electronic

structure of the dye (core,  $\pi$ -conjugated system, end groups), we also investigated related dyes having a similar core but bearing electron-accepting end groups (**2**) or without end groups (**3**). An extended version of **1** having an elongated  $\pi$ -conjugated system was also investigated (**4**) as well as a more compact version (without thiophene moieties in the  $\pi$ -conjugated system) built from a truxene (i.e., with three fused fluorene units) core having different symmetry (**5**). We thus synthesized a series of new dyes (Scheme 2) and analyzed their electrochemical and ECL properties in organic solvent. All these features could be of interest for biosensing if combined with the benefits of nanoconfinement.

## Results and Discussion

### Electrochemistry

The electrochemical properties of all the spirofluorene-based and truxene-based dyes were investigated by cyclic voltammetry (Figure 1, Table 1). These experiments were performed at a platinum working electrode in dichloromethane that contained 1 mM of each dye and 0.1 M *n*-tetrabutylammonium hexafluorophosphate (TBAPF<sub>6</sub>) as supporting electrolyte. As shown in Figure 1, the cyclic voltammogram (CV) of **1** exhibits three reversible oxidation waves, at  $E_{1,\text{ox}} = 0.89 \text{ V}$ ,  $E_{2,\text{ox}} = 1.24 \text{ V}$ , and  $E_{3,\text{ox}} = 1.50 \text{ V}$  versus SCE. The peak current of the first oxidation wave is nearly twice that of the other two waves. This is probably related to a two-electron-transfer reaction occurring in the first wave and one-electron-transfer reactions in the next two waves. The first oxidation wave can be attributed to formation of the dication radical by simultaneous oxidation of the two triphenylamine moieties.<sup>[4c, 13a, 25]</sup> This two-electron wave, which generates triphenylaminium dication derivatives, indicates that the electronic communication between the two terminal triphenylamine groups is negligible.<sup>[13a, 25a]</sup> The influence of the scan rate on the oxidation waves was studied in



**Scheme 2.** Synthesis of dyes **1**, **2**, **3**,<sup>[26]</sup> **4**, and **5**. a) 1,4-Dibromobutane, KOH, *n*Bu<sub>4</sub>NBr, toluene, 75 °C, 2.5 h (80% of **B**). b) 5-Formyl-2-thienylboronic acid, K<sub>2</sub>CO<sub>3</sub>, [PdCl<sub>2</sub>(dppf)] (dppf = 1,1'-bis(diphenylphosphino)ferrocene), MeOH/toluene, 75 °C, 20 h (94% of **2**). c) 2-Thienylmagnesium bromide, [PdCl<sub>2</sub>(dppf)], THF, reflux 48 h (75% of **3**). d) **3**, *N*-Iodosuccinimide, CHCl<sub>3</sub>/glacial acetic acid, 90 °C, 5 min (99% of **C**). e) **C**, 4-(*N,N'*-Diphenylamino)phenylboronic acid, [PdCl<sub>2</sub>(dppf)], K<sub>2</sub>CO<sub>3</sub>, MeOH/toluene, 74 °C, overnight (61% of **1**). f) **2**, *t*BuOK, 4-(*N,N'*-dibutylaminobenzyl)triphenylphosphonium iodide, CH<sub>2</sub>Cl<sub>2</sub>, RT, 24 h (71% of **4**). g) K<sub>2</sub>CO<sub>3</sub>, Cu<sub>6</sub>I<sub>8</sub>, 18-crown-6, diphenylamine, *o*-dichlorobenzene, reflux, 60 h (77% of **5**).

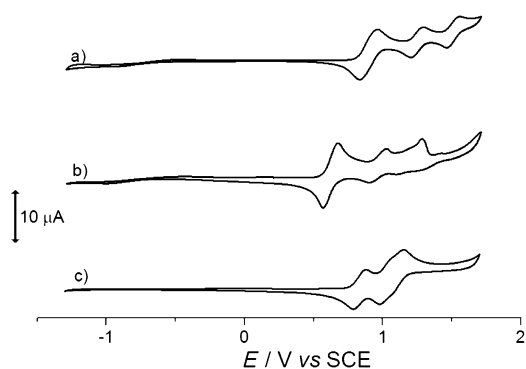


**Figure 1.** CVs of a) a 1 mM solution of **1**, b) a 1 mM solution of **4**, and c) a 1 mM solution of **5** in CH<sub>2</sub>Cl<sub>2</sub> with 0.1 M TBAPF<sub>6</sub> as supporting electrolyte. A Pt disk and a Ag wire were used as working electrode and pseudoreference electrode, respectively. The potential was calibrated with Fc/Fc<sup>+</sup> (0.342 V vs. SCE). Scan rate: 100 mV s<sup>-1</sup>.

the range from 0.05 to 1 V s<sup>-1</sup> (Supporting Information, Figure S1) and the current peak shows linear evolution with respect to the square root of the scan rate (Supporting Information, Figure S2). This demonstrates a diffusion-controlled process on the Pt surface in this potential window for all three well-separated anodic steps. The next two reversible anodic one-electron waves are consistent with oxidation of the central spirofluorene core.<sup>[4c, 13a, 25b]</sup> However, another hypothesis that cannot be excluded is that the reversible one-electron oxidation waves are related to oxidation of the thiophene moieties. Whatever, it shows that the cation **1**<sup>4+</sup> is stable in solution during at least the timescale of the voltammetric experiments. We have not observed the reduction of **1** in the explored potential window accessible in CH<sub>2</sub>Cl<sub>2</sub>. However, with the goal of obtaining bright ECL luminophores, the reversible oxidation behavior should allow ECL generation following the oxidative/

**Table 1.** Electrochemical and photophysical properties of **1**, **4** and **5** in CH<sub>2</sub>Cl<sub>2</sub>.

Compound	$E_{1,ox}^{[a]}$ [V]	$E_{2,ox}^{[a]}$ [V]	$E_{3,ox}^{[a]}$ [V]	$\lambda_{max}^{Abs}$ [nm]	$\lambda_{max}^{FL}$ [nm]	$\lambda_{max}^{ECL}$ [nm]	$E_{FL}^{[b]}$ [eV]	$\Delta G^{\circ [c]}$ [eV]	$\Phi_{FL}^{[d]}$	$\Phi_{ECL}^{[e]}$
<b>1</b>	0.89	1.24	1.50	415	474, 496	503	2.50	-0.49	0.71	4.54
<b>4</b>	0.61	0.95	1.27 <sup>[f]</sup>	447	546	549	2.27	-0.42	0.67	1.11
<b>5</b>	0.83	1.05 <sup>[g]</sup>	1.15 <sup>[g]</sup>	360	388	- <sup>[h]</sup>	3.20	0.40	0.40	0.05

[a] Oxidation potentials (vs. SCE) calculated as the mean value of the redox peaks. [b]  $E_{FL}$ : energy of the excited singlet state estimated from fluorescence emission maximum (Supporting Information, Figure S5) with Equation (10). [c] The values of  $\Delta G^{\circ}$  were calculated by using Equation (9). [d] Fluorescence quantum yields in CH<sub>2</sub>Cl<sub>2</sub> were determined by using fluorescein for **1** and quinine bisulfate for **4** and **5**. [e] The ECL efficiency was calculated by comparison with [Ru(bpy)<sub>3</sub>]<sup>2+</sup> as reference ( $\Phi_{ECL} = 1$ ). [f] Anodic wave not well defined with loss of reversibility. [g] Partially overlapping anodic waves. [h] ECL signal too weak to allow recording of the ECL spectrum.

reductive pathway with tri-*n*-propylamine (TPrA) as co-reactant.<sup>[15a,27]</sup>

Further electrochemical experiments were performed on **2** and **3** to investigate the influence of the end groups on the electrochemical properties. We recorded the CV of **3**, which is an intermediate in the synthesis of **1**. The CV shows the irreversible oxidation waves of the thiophene moieties and the first anodic peak potential at 1.26 V versus SCE (Supporting Information, Figure S3). We also studied **2**, which is similar to **1**, but instead of electron-donor groups (i.e., triphenylamine), is terminated by an aldehyde group, which is known to be a good electron-withdrawing group.<sup>[28]</sup> By changing the nature of the end group from donor to acceptor, one would reasonably expect a shift of both the reduction and the oxidation waves to more positive (or less negative) values. As depicted in Figure S4 of the Supporting Information, the CV of dye **3** in CH<sub>2</sub>Cl<sub>2</sub> shows an irreversible oxidation at high potential ( $E_{ox} = 1.6$  V vs. SCE). The results obtained for both **2** and **3** are comparable to the wave observed at 1.31 V versus SCE for the electropolymerization of thiophene moieties.<sup>[29]</sup> After only a single scan, polymer films were observed on the Pt surface. This kind of electropolymerization is not of interest in present study, but provides evidence that the two end thiophene moieties exhibit high electrochemical and chemical reactivity in **3** and also in **2**. The drastic change in oxidation behavior between **1** and both precursors shows that the substitution with the terminal electron-donor triphenylamine moiety in the  $\alpha$  position prevents its oxidation through these positions and subsequent polymerization.

Similar to **1**, dye **4** which has an alkene connector between the thiophene moiety and the terminal donor groups (i.e., dibutylamino groups), shows a first two-electron reversible oxidation wave and a one-electron oxidation wave. The first two oxidation potentials  $E_{1,ox}$  and  $E_{2,ox}$  of **4** are shifted to less anodic potentials by about 300 mV in comparison to **1** (Table 1). Indeed, the butyl chain is known to be a stronger electron-donor moiety than diphenyl.<sup>[28]</sup> This donor effect may also be reinforced by the alkene group placed between the thiophene groups and the terminal groups. It makes the molecule much easier to oxidize and can stabilize the radical cation by charge delocalization. The subsequent oxidation processes are more complex and reveal the presence of features that are characteristic of irreversibility. They consist of a shoulder at 1.18 V before a mainly irreversible wave at 1.27 V versus SCE. The irreversibility of **4** at potentials above  $E_{2,ox}$  remains so far unclear but it points to the instability of the corresponding electrogenerated radicals, most probably of the spirofluorene core, due to the presence of the alkene moiety, which may be responsible for isomerization processes. Whatever, this characteristic may provide some insight into the comparative studies on the ECL efficiency of the different compounds (see below).

The electrochemical properties of the electron-donating diphenylamine groups were also examined by studying compound **5**, which mainly consists of three diphenylamine moieties grafted on a truxene core. Interestingly, the CV of **5** shows three reversible oxidation waves: the first occurs at 0.83 V versus SCE and the last two partially overlap. Considering the

chemical structure, these three waves are consistent with the oxidation of the terminal diphenylamine moieties. The fact that they are partially separated indicates that the electronic communication between the terminal diphenylamine groups is non-negligible, in contrast to what is observed for **1**. The reversibility also points to good stability of the trication  $5^{3+}$ . In fact, the reversibility dominates the entire oxidation processes of the analyzed compounds, especially **1**. Stability of the electrogenerated luminophore radicals is of fundamental importance to produce high ECL intensity.<sup>[22n]</sup>

### Spectroelectrochemistry

In situ spectroelectrochemical studies on **1** were performed in solution to evaluate the spectral changes between the neutral and first oxidized state (i.e.,  $E_{1,ox}$ ). This is of importance for studying in more detail the oxidation process and the stability of the radicals, which is essential for the ECL efficiency. It also allows their suitability as electrofluorochromic and electrochromic materials to be assessed.<sup>[30]</sup> The dye was dissolved in a 0.1 M solution of TBAPF<sub>6</sub> in CH<sub>2</sub>Cl<sub>2</sub>, and the absorption and emission spectroelectrochemical studies were done with a Pt-mesh working electrode. At the first oxidation potential  $E_{app} = 0.8$  V versus Ag/Ag<sup>+</sup>, the evolution of the UV/Vis and fluorescence spectra with time was recorded (Figure 2). Interestingly, monitoring of the absorption revealed modification of the electronic transition when the first oxidized state is reached. As shown in Figure 2a, the periphery-to-core intramolecular charge-transfer (ICT) band<sup>[31]</sup> of **1** in CH<sub>2</sub>Cl<sub>2</sub> at 415 nm vanished on oxidation and a new redshifted absorption band appeared at 610 nm. The evolution of the fluorescence band at 496 nm is a good mirror image of that of the absorption band at 415 nm. This observation may be attributed to the reversal of ICT (i.e., core-to-periphery ICT transition) due to the strongly electron withdrawing character of triphenylaminium end groups generated after loss of electrons from the triphenylamine moieties.<sup>[30b]</sup> After approaching equilibrium, an open-circuit potential ( $E = 0$  V versus Ag/Ag<sup>+</sup>) was applied to the system. The absorbance recovered with time until the intensity and shape of the curve were as same as the initial state. This confirms the reversibility observed by cyclic voltammetry for the oxidation process. A similar finding was made by fluorescence studies. The fluorescence intensity showed reversible variation during the oxidation and recovery processes on excitation at 415 nm (Figure 2b). We also excited **1** at the new absorption band that appeared at 600 nm. However, this did not lead to any fluorescence emission during the oxidation process (Supporting Information, Figure S6). This is consistent with an excited state having quinoidal character (in relation with strong core-to-periphery ICT) resulting in very low fluorescence quantum yield. Therefore, the absorption and fluorescence properties of **1** are also controlled by these terminal electron-donating triphenylamine groups.

Besides, thanks to this totally reversible oxidation behavior, a different method to determine the half-wave potential  $E_{1/2}$  and number  $n$  of electrons for the first oxidation process was applied on the basis of the spectroelectrochemical studies dis-

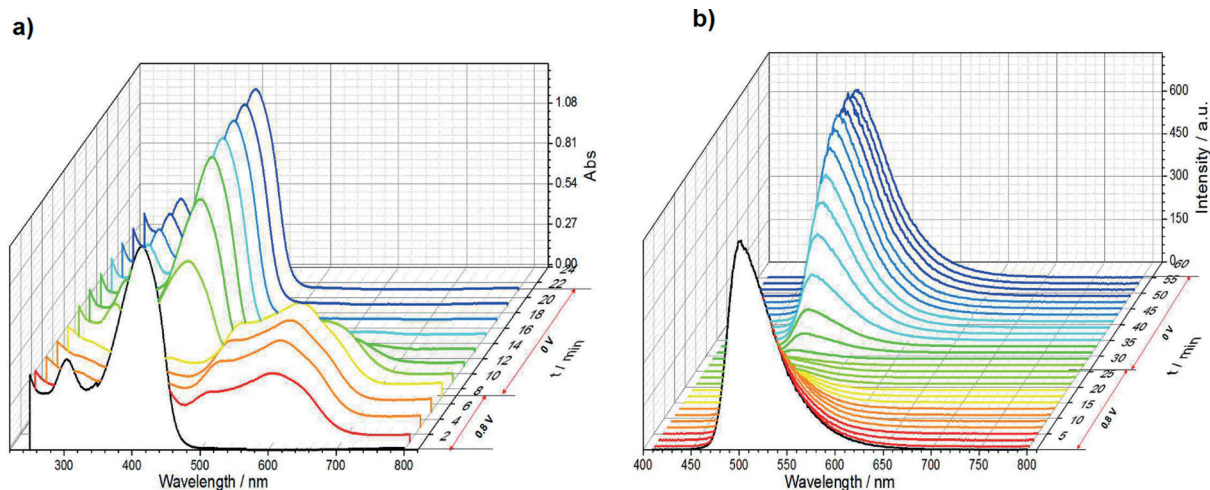


**Figure 2.** Time-resolved a) UV/Vis and b) fluorescence spectra ( $\lambda_{\text{ex}} = 415 \text{ nm}$ ) for **1** under oxidation at 0.8 V versus Ag/Ag<sup>+</sup> and electrochemical restoration by applying  $E = 0 \text{ V}$  versus Ag/Ag<sup>+</sup> in CH<sub>2</sub>Cl<sub>2</sub> solution containing 0.1 M TBAPF<sub>6</sub>.

cussed above.<sup>[32]</sup> A series of oxidation potentials was applied in CH<sub>2</sub>Cl<sub>2</sub> in a thin-layer cell, and individual UV/Vis or fluorescence spectra were recorded after applying an anodic potential during the time required to obtain equilibrium. As shown in Figure 2, the absorbance and the fluorescence decay in a similar way when more anodic potentials are imposed. The absorbance ( $\lambda_{\text{max}}^{\text{Abs}} = 415 \text{ nm}$ ) and fluorescence ( $\lambda_{\text{max}}^{\text{FL}} = 496 \text{ nm}$ ) variations can be related to the ratio of the oxidized (O) state to the reduced (R) state at different holding potentials by Equations (1) and (2):

$$[R]/[O] = [A_2 - A_3]/[A_1 - A_2] \quad (1)$$

$$E_{\text{app}} = E_{1/2} - (0.0591/n) \lg([R]/[O]) \quad (2)$$

where  $A_2$  is the absorbance measured at a wavelength at a given potential and  $A_1$  and  $A_3$  are the absorbances of the totally reduced and oxidized species, respectively. According to the Nernst equation, a plot of  $E_{\text{app}}$  versus  $\lg([R]/[O])$  is linear with a slope of  $0.0591/n$  and an intercept of  $E_{1/2}$ . The potential-

resolved UV/Vis spectra are shown in Figure 3a, in which the inset shows a plot of  $E_{\text{app}}$  versus  $\lg([R]/[O])$ . The linear fitting gives a slope of  $-0.028$  and an intercept of 0.70 V (Figure 3a, inset), that is, the number of electrons transferred is two and  $E_{1/2}$  is 0.70 V for the first oxidation reaction. We performed a similar treatment of the potential-resolved fluorescence data with  $A_1$ ,  $A_2$ , and  $A_3$  having the same meaning as above, except that they correspond to the fluorescence intensities measured at 496 nm (Figure 3b). For the fluorescence, a slope of  $-0.030$  and  $E_{1/2} = 0.71 \text{ V}$  were found (Figure 3b, inset). These results confirmed a two-electron-transfer reaction occurring at the first oxidation wave and the stability of the oxidized resulting dications for several minutes. It also demonstrates that the two following oxidation waves correspond to a one-electron transfer reaction.

### ECL of the luminophores

ECL of spirofluorene derivatives has essentially been generated by the annihilation mechanism or via the reductive/oxidative pathway by applying a cathodic potential in presence of ben-

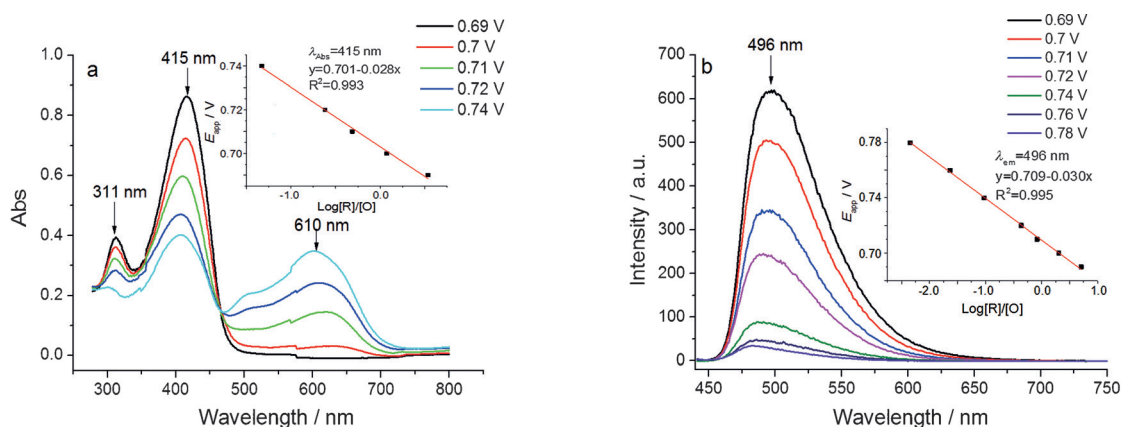


**Figure 3.** Evolution of the a) UV/Vis and b) fluorescence spectra ( $\lambda_{\text{ex}} = 415 \text{ nm}$ ) for **1** when applying different potentials during the first oxidation process in CH<sub>2</sub>Cl<sub>2</sub> solution containing 0.1 M TBAPF<sub>6</sub>. Insets are plots of  $E_{\text{app}}$  versus  $\lg([R]/[O])$ .

zoyle peroxide as a cathodic coreactant.<sup>[4c,18,25,33]</sup> In the present work, we exploited the good stability of the oxidized forms of **1**, and ECL of the luminophores was thus tested with an anodic sacrificial coreactant. In this case, TPrA was used as coreactant in order to follow the oxidative/reductive pathway, and the excited state was generated after simultaneous oxidation of TPrA and of the tested luminophore (Figure 4). To this end, we imposed anodic potentials in TPrA solution by scanning the potential up to 1.7 V versus SCE.

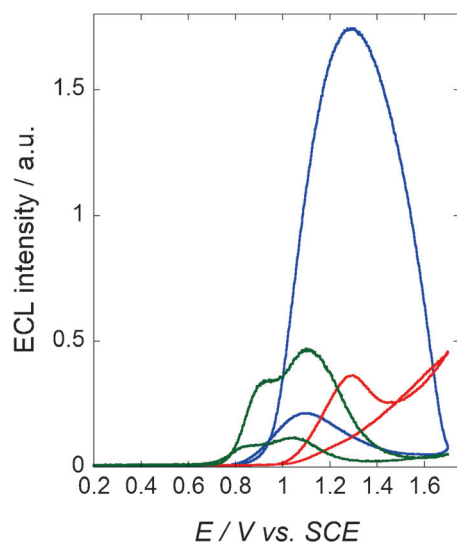


**Figure 4.** Comparison of the ECL signals for a) **1** (blue line), b) **4** (green line), and the  $[\text{Ru}(\text{bpy})_3]^{2+}$  reference (red line). ECL was recorded with a glassy carbon electrode in  $\text{CH}_2\text{Cl}_2$  solution containing 1 mM luminophore, 0.1 M  $\text{TBAPF}_6$ , and 100 mM TPrA. Scan rate:  $100 \text{ mV s}^{-1}$ .

The ECL signal of **1** starts to increase at 0.9 V, reaches a maximum at 1.29 V, and then decreases until 1.7 V versus SCE (Figure 4). The ECL emission was very intense and extended over a large potential range compared to the reference compound  $[\text{Ru}(\text{bpy})_3]^{2+}$  (bpy = 2,2'-bipyridine; Supporting Information, Figures S7–S9). In addition, it is noteworthy that ECL is generated just after the first two-electron oxidation wave corresponding to simultaneous oxidation of the two terminal triphenylamine moieties, but it starts before the second oxidation wave (Supporting Information, Figure S10). Since the TPrA coreactant is already oxidized at 0.8 V versus SCE (Supporting Information, Figures S7–S9), it is not the limiting step in the ECL process. In a similar way, the ECL signal of **4** increases at 0.75 V versus SCE and is composed of two overlapping peaks with a maximum at 1.1 V versus SCE. Afterwards, it decays very rapidly. The ECL emission occurring at lower anodic potential is consistent with the shift of the first oxidation wave to less anodic potential for **4** in comparison to **1**. For both compounds, ECL is thus generated after the two-electron oxidation of the end-capping donor groups, but 200 mV before the second oxidation wave (Supporting Information, Figure S10). The different shapes of the ECL responses in Figure 4 can be explained by considering the widths at half-maximum of the ECL peaks, which are 450, 380, and 180 mV for **1**, **4**, and

$[\text{Ru}(\text{bpy})_3]^{2+}$ , respectively. The ECL signal extends over a much larger potential range for both spirofluorene dyes in comparison with  $[\text{Ru}(\text{bpy})_3]^{2+}$ . There is thus a clear correlation between the oxidation behavior and both the position and the extension of the potential domain in which ECL is generated. An explanation for this intriguing behavior could be that the third oxidation wave contributes partially to the ECL process giving high ECL intensity due to the remarkable stability of the corresponding cationic species. Ding et al. reported the self-enhanced ECL of an iridium-based complex, the ECL efficiency of which increased after each oxidation step.<sup>[22]</sup> However, in their case, self-enhancement of ECL involved oxidation of dimethylamino groups on the bipyridine ligands of the iridium complex, which act as a self-coreactant.<sup>[22]</sup> The cascade of reactions leading ultimately to the ECL emission could be described by the following mechanism [Eqs. (3)–(8)]:



where  $\text{Im}^+$  is the iminium product.

Both TPrA and **1** (or **4**) are oxidized at the electrode surface. Then the cation radical  $\text{TPrA}^{+\cdot}$  undergoes a deprotonation step, which produces a strongly reducing  $\text{TPrA}^{\cdot}$  radical. This intermediate reacts with the oxidized organic dye  $\mathbf{1}^{3+}$  to generate its excited state  $\mathbf{1}^*$ . Finally, it relaxes to the ground state and emits light.<sup>[16,34]</sup> The calculation of the ECL efficiency  $\Phi_{\text{ECL}}$  is detailed in the Supporting Information, and the corresponding results are collected in Table 1. The ECL signal was recorded by scanning the potential of a glassy carbon electrode from 0 to +1.5 V versus SCE in a  $\text{CH}_2\text{Cl}_2$  solution containing 0.1 M TPrA and 0.1 M  $\text{TBAPF}_6$  (Supporting Information, Figures S7–S9). The ECL efficiency  $\Phi_{\text{ECL}}$  depends mainly on the generation of the excited state [Eq. (7)] and subsequent radiative emission to return to the ground state [Eq. (8)]. Therefore, it is governed by two main contributions: the thermodynamics of reaction (7) ( $\Delta G^\circ$ ) and the photophysics of the radiative de-excitation ( $\Phi_{\text{FL}}$ ). The free energy  $\Delta G^\circ$  can be calculated from Equations (9) and (10):

$$\Delta G^\circ = E_{\text{red}}^\circ(\text{TPrA}^{\cdot}) - E_{2,\text{ox}} + E_{\text{FL}} \quad (9)$$

$$E_{\text{FL}} = hc/\lambda_{\text{max}}^{\text{FL}} = 1239.81/\lambda_{\text{max}}^{\text{FL}} \quad (10)$$

where  $E_{\text{red}}^\circ(\text{TPrA}^{\cdot})$ , the reduction potential of the TPrA neutral radical, has previously been found to have a value of  $-2.1 \text{ V}$ .<sup>[16,35]</sup> Since ECL is mainly emitted at the level of the second oxidation wave, we employed the corresponding potential  $E_{2,\text{ox}}$  in Equation (9). Considering the values of  $E_{2,\text{ox}}$  and

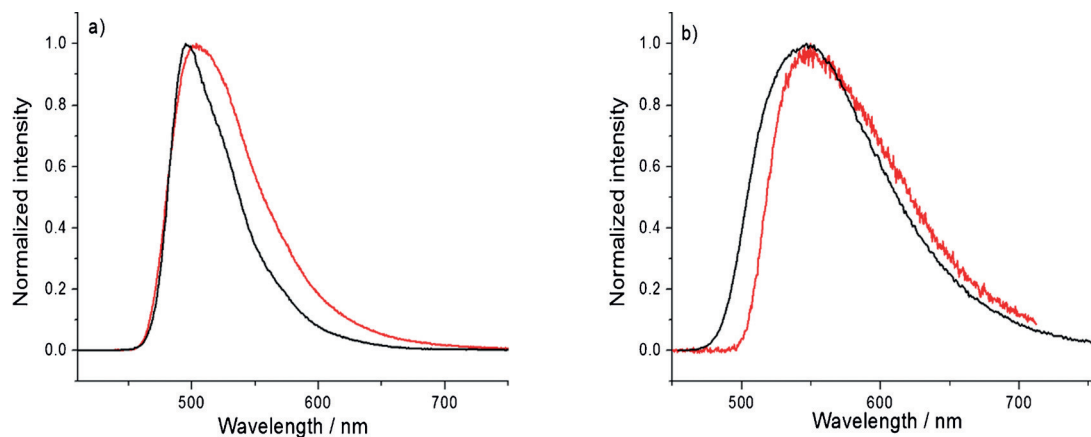
of  $E_{FL}$  in Table 1, one can see clearly that reaction (7) provides enough energy for compounds **1** and **4** to populate the excited state, whereas this energy is insufficient for **5**. This explains why **5** gives very little or no ECL. Dye **1** showed very bright ECL and its efficiency is 4.5 times greater than that of reference compound  $[Ru(bpy)_3]^{2+}$ . The value obtained is remarkably high as compared to those observed in other organic ECL dyes and fluorene compounds.<sup>[4c, 18, 25, 33, 36]</sup> From an energetic point of view, the reaction between the dication radical  $1^{2+}$  and TPrA $^{\cdot}$  would also be exergonic enough to populate the first singlet excited state  $1^*$ . Indeed, if we use the value of  $E_{1,ox}$  in Equation (9), the available energy is sufficient by about 0.14 eV and 0.08 eV for **1** and **4**, respectively, to populate the excited state and to generate ECL. This means that there is another photochemical process that quenches the ECL emission until both donor groups are oxidized. Since the fluorescence quantum yields are relatively similar for **1** and **4** (0.71 and 0.67, respectively), the important difference for the ECL efficiency between the two dyes may be due to the more exergonic reaction generating the excited state and to the higher stability of the oxidized cation radicals. Reaction (7) is actually energy-sufficient by about 0.49 and 0.42 eV according to Equation (9) for **1** and **4**, respectively. This slightly higher available energy cannot justify such an important difference in the efficiency of the ECL process. Nevertheless, the higher stability of the oxidized forms<sup>[22n]</sup> explains this remarkable characteristic, as shown in the voltammetric studies.

Thanks to their strong ECL emission, ECL spectra for **1** and **4** could be recorded (Figure 5). The ECL signal of **5** was too weak to allow recording of its ECL spectrum. By comparison with the

corresponding fluorescence spectra, redshifts were observed in ECL spectra (7 nm for **1** and 3 nm for **4**). Such redshifts are common in ECL and are caused by the inner filter effect due to the high concentration of chromophores used in ECL experiments.<sup>[25b, 37]</sup> Nonetheless, these results confirmed that the same excited state  $1^*$  were produced by photochemical and electrochemical excitation.

### Electrochemistry and ECL of FONs

Fluorescent organic NPs, and more particularly fluorene-based NPs,<sup>[13a, 37a, 38]</sup> have been the subject of relatively few reports describing their electrochemical and ECL properties compared to inorganic NPs.<sup>[22a, c, d, 39]</sup> To investigate their characteristics in comparison with the molecular compounds, FONs were prepared in aqueous solution by the nanoprecipitation method<sup>[40]</sup> according to a reported procedure.<sup>[23]</sup> More precisely, FONs were obtained by fast addition of a minute amount of a stock solution of the corresponding dye in THF to a large amount of water under sonication. Instantly after addition, colored, non-turbid solutions are obtained that show intense absorption in the near-UV/violet region, indicating the formation of NPs. Furthermore, under UV irradiation, the suspensions in water emit strong fluorescence in the visible region (Supporting Information, Figure S5) attesting to the formation of FONs. FONs [**1**] emit in the green region and FONs [**4**] emit in the yellow region (Table 2), and both are ultrabright. The elongated  $\pi$ -conjugated system of dye **4** is responsible for the redshifted absorption and emission of FONs [**4**] compared to those made from dye **1**. Both FONs exhibit good colloidal and structural



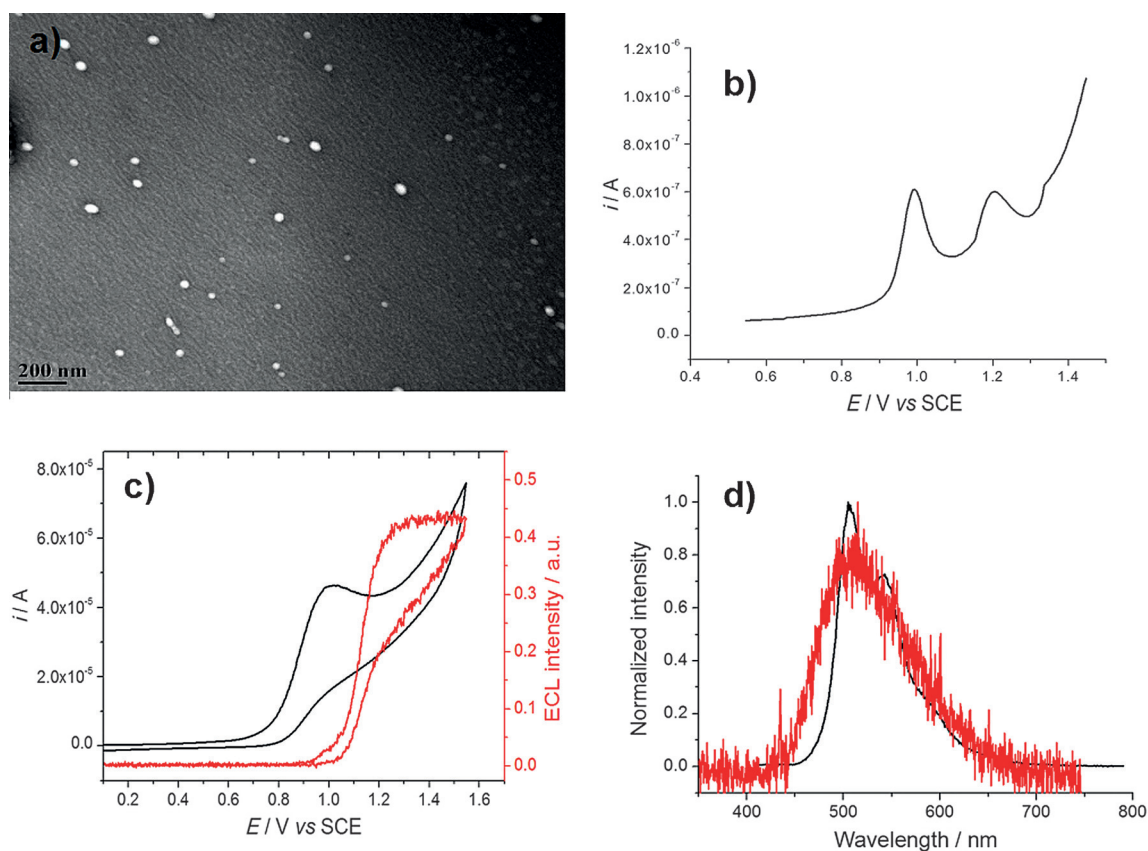
**Figure 5.** Normalized fluorescence (black line) and ECL spectra (red line) for a) **1** and b) **4** in  $CH_2Cl_2$ . ECL spectra were recorded in  $CH_2Cl_2$  solution containing 0.1 M TBAPF $_6$  with 100 mM TPrA as a co-reactant.

Table 2. Structural and luminescence (fluorescence and ECL) characteristics of FONs.									
	$d_{TEM}$ [nm] <sup>[a]</sup>	$d_h$ [nm] <sup>[b]</sup>	$\zeta$ [mV] <sup>[c]</sup>	$\lambda_{max}^{Abs}$ [nm]	$\epsilon_{max}$ [10 <sup>9</sup> M <sup>-1</sup> cm <sup>-1</sup> ]	$\lambda_{max}^{FL}$ [nm]	$\Phi_{FL}^{[d]}$	$\epsilon_{max} \Phi_{FL}$ [10 <sup>8</sup> M <sup>-1</sup> cm <sup>-1</sup> ] <sup>[e]</sup>	$\lambda_{max}^{ECL}$ [nm]
[ <b>1</b> ]	43	103	-70	400	1.6	507	0.14*	2.2	510
[ <b>4</b> ]	43	68	-50	426	2.1	560	0.02**	0.42	-

[a] Diameter of the FONs determined by TEM. [b] Hydrodynamic diameter derived from DLS experiment. [c] Zeta potential. [d] Fluorescence quantum yields were determined by using fluorescein\* or cresyl violet\*\*. [e] Brightness.

stability in water, as evidenced by monitoring over time the evolution of the absorption and fluorescence spectra (Supporting Information, Figure S13). The size and morphology (spherical shape) of the FONs were characterized by TEM (Table 2). The good colloidal stability of the FONs is further attested to by their large negative zeta potentials. We note that the hydrated radii determined by dynamic light scattering in water are somewhat larger than those measured for “naked” nanoparticles by TEM. This difference can be ascribed to the highly negative surface potentials of both FONs, which is responsible for the presence of a shell of H-bonded water molecules.<sup>[23]</sup> The thickest bound water shell is obtained for the FONs having the more negative potential (i.e., FONs [1]). The fluorescence quantum yields of the FONs are significantly reduced in comparison to those of individual dyes in CH<sub>2</sub>Cl<sub>2</sub> solution (see Tables 1 and 2). This can be related to both a decrease of the radiative decay rate (in relation with excitonic coupling between dye subunits within FONs) and increase in nonradiative decay rate. This can be attributed to the presence of water molecules strongly bonded to the FON surface, which provide efficient nonradiative vibrational decay channels. Yet, both FONs retain fluorescence, and due to their huge absorption coefficient (Table 2), they show high brightness, typically orders of magnitude larger than those of quantum dots or even dyed silica nanoparticles.<sup>[41]</sup>

Since FONs [1] and [4] are stable in water, the electrochemical characterization of these FONs was performed in 100 mM phosphate-buffered saline (pH 7.4). Differential pulse voltammetry (DPV) of FONs [1] dispersed in buffer solution showed two oxidation peaks at 0.99 and 1.20 V versus SCE and one small shoulder at 1.33 V versus SCE (Figure 6b). The last-named is not well defined, because water oxidation starts in the same potential region. As mentioned above, **1** exhibits three oxidation waves, at  $E_{1,ox} = 0.89$  V,  $E_{2,ox} = 1.24$  V, and  $E_{3,ox} = 1.50$  V versus SCE. Thus, there is good agreement between the molecular and NP forms of **1**. In addition, the current of the first anodic peak is nearly twice that of the second one for FONs [1]. It thus corresponds to sequential two- and one-electron-transfer reactions for the first two peaks, as demonstrated by cyclic voltammetry and spectroelectrochemistry. This is more difficult to determine for the third peak due to its shape. In any case, the DPV results show that both the triphenylamine terminal moieties and the spirofluorene core are electrochemically accessible in the FONs [1]. DPV of FONs [4] exhibited only a one small oxidation wave, which starts at 0.9 V and finishes at 1.3 V versus SCE (Supporting Information, Figure S11a). However, although DPV is a differential technique allowing better resolution of peak current than cyclic voltammetry, it is difficult to identify specific peaks and to attribute them in this particular case.



**Figure 6.** a) TEM image of FONs [1] dispersed in water. b) DPV of 0.4 nM FONs [1] in 100 mM phosphate-buffered saline (PBS, pH 7.4) solution. (c) Voltammetric and ECL curves of 0.4 nM FONs [1] in 100 mM PBS (pH 7.4) containing 100 mM TPrA. Scan rate: 100 mV s<sup>-1</sup>. d) Fluorescence (black line) and ECL (red line) spectra of FONs [1] in 100 mM PBS (pH 7.4) with 100 mM TPrA.

Then ECL emission was generated in a buffer solution containing both the FONs and TPrA when the electrode potential was scanned from 0 to 1.5 V versus SCE. As detailed in the cascade of reactions (3)–(8), the oxidized NPs reacted with the strongly reducing radical TPrA<sup>•</sup> to populate the excited state and eventually emit the ECL signal. As shown in Figure 6c for FONs [1], ECL intensity started to increase at 0.95 V and reached a plateau at 1.5 V versus SCE. FONs made from **1** thus behave in water like **1** in organic solution and generate ECL after oxidation of the terminal triphenylamine moieties. This means that the oxidized FONs react with the neutral TPrA<sup>•</sup> radical to generate the excited state in the NPs. For FONs made from dye **4**, after a similar initial increase, the ECL intensity decreases very rapidly (Supporting Information, Figure S11b). This behavior is consistent with the ECL study on the molecular species, whereby ECL of **4** decreases rapidly, whereas it lasted over a larger potential range for **1**.

The ECL efficiency of the FONs was calculated by comparison with [Ru(bpy)<sub>3</sub>]<sup>2+</sup>/TPrA as reference ( $\Phi_{\text{ECL}} = 100\%$ ). At a scan rate of 100 mVs<sup>-1</sup>, the values of  $\Phi_{\text{ECL}}$  were 20.8 and 5.5% for FONs [1] and [4], respectively. Such a ratio between the two FONs is consistent with the ECL efficiencies of the molecular compounds reported in Table 1. It shows that nanoconfinement did not modify their respective ECL properties in comparison with the molecular forms. The ECL efficiency depends on the scan rate<sup>[42]</sup> and the reported values are particularly high. For example, Hesari et al. reported recently the ECL efficiency of BODIPY-capped PbS.<sup>[42]</sup> At the same scan rate (i.e. 100 mVs<sup>-1</sup>), they obtained values between 8 and 10%, which are the highest ECL efficiencies observed for semiconductor nanocrystals. Au nanoclusters provided an even higher ECL efficiency of 103%.<sup>[43]</sup>

The ECL signal of FONs [1] was strong enough to allow the ECL spectrum (Figure 6d) to be recorded. Comparison with the corresponding fluorescence spectrum clearly shows the similarity between photoluminescence and ECL spectra (Figure 6d), which confirms that the same excited state is reached by both excitation methods. Unfortunately, the ECL intensity of FONs [4] is too low to allow an ECL spectrum to be acquired. This emphasizes that the choice of suitable dye subunits is critical to achieve stable and ultrabright FONs that are also capable of generating ECL in water. As such, the fully organic nanoparticles, easily prepared from the quadrupolar spirofluorene dye having triphenylamine terminal moieties **1**, have major promise for bioimaging and sensing purposes.

## Conclusion

We synthesized and characterized a series of symmetric luminophores with blue to yellow emission built from a spirofluorene core connected to terminal donor or acceptor groups via  $\pi$ -conjugated linkers having thiophene moieties. Only quadrupolar derivatives having donor end groups (luminophores **1** and **4**) show reversible oxidation waves. In contrast, a related dye based on direct grafting of three diarylamino groups to a truxene core shows three successive one-electron oxidation steps, and this shows that the nature of the core and conjugat-

ed system influence the communication between the peripheral electroactive donor moieties. Interestingly only quadrupolar derivatives having donor end groups exhibit intense ECL. The most efficient ECL is achieved with green-emitting **1**, which exhibits three reversible oxidation waves with highly stable oxidized states (**1**<sup>2+</sup>, **1**<sup>3+</sup>, **1**<sup>4+</sup>). The  $\pi$  conjugation with the thiophene direct connector allows charge delocalization and the stabilization of the electrogenerated cation radicals. The stability of the oxidized radicals results in remarkably high ECL efficiency for this luminophore with TPrA as coreactant. It is 4.5 times higher than that of the model compound [Ru(bpy)<sub>3</sub>]<sup>2+</sup> with a very intense and large ECL signal which may involve cumulative contributions of the higher oxidized states. In addition, we found that ECL is only emitted after the oxidation of the end-capping (triarylamino) donors. Redox and ECL behaviors of the FONs are consistent with those of the corresponding molecular species. The molecular confinement of these luminophores in fluorescent nanoparticles does not change the electrochemical and ECL properties of the FONs, which are very bright nanoemitters. In conclusion, the investigated compounds demonstrate the possibility to design highly efficient green-emitting molecular species and organic NPs for ECL applications.

## Experimental Section

### Materials

Compounds **A**,<sup>[44]</sup> **1**,<sup>[23]</sup> and **D**<sup>[45]</sup> were prepared according to literature procedures.

### General methods

Commercially available reagents were used without further purification. Dry solvents were distilled from the appropriate drying reagents prior to use. All air- or water-sensitive reactions were carried out under argon. Reactions were monitored by performing TLC on Merck silica gel precoated aluminum sheets (60F-254). Column chromatography was performed with Fluka silica gel Si 60 (40–63  $\mu\text{m}$ , 230–400 mesh). Melting points were determined with a Kofler bench. The IR spectrum of **2** was recorded with a PerkinElmer Spectrum 100 Optica spectrometer. <sup>1</sup>H and <sup>13</sup>C NMR spectra were recorded with a Bruker Avance I 300 spectrometer at 300 and 75 MHz respectively or with a Bruker Avance II spectrometer at 400 and 100 MHz respectively. <sup>1</sup>H chemical shifts are reported in parts per million relative to TMS as internal standard. <sup>13</sup>C chemical shifts are given relative to the central peak of CDCl<sub>3</sub> at 77.0 ppm. High- and low-resolution mass spectra were recorded at the Centre Régional de Mesures de l'Ouest (C.R.M.P.O., Rennes) by using QTOF II or MicroTOF-Q II instruments for **B**, **2**, and **4** and at CESAMO (Bordeaux, France) for **3** and **5**. Elemental analyses were performed at CESAMO (Bordeaux, France) or at I.C.S.N.-C.N.R.S. (Gif-sur-Yvette, France).

### Synthesis

**2,7'-Diiodospiro[cyclopentane-1,9'-fluorene] (B)**: *n*Bu<sub>4</sub>NBr (0.21 g, 0.65 mmol) in 1,4-dibromobutane (12.0 mL, 100.60 mmol) was added to a solution of KOH (26.81 g, 477.81 mmol) in water (26.8 mL), and the mixture stirred at 75 °C for 30 min. A solution of 2,7-diiodofluorene (4.00 g, 9.57 mmol) in toluene (26.0 mL) was

added and the reaction mixture was stirred at 75 °C for 2 h. After addition of water, extraction with CH<sub>2</sub>Cl<sub>2</sub>, and drying over MgSO<sub>4</sub>, the organic layer was filtered through a short pad of silica and the solvent evaporated. The crude compound was recrystallized by slow cooling of a saturated solution in hot heptane to yield 3.62 g (80%) of **B** as pale cream crystals. <sup>1</sup>H NMR (CDCl<sub>3</sub>, 300 MHz): δ = 7.73 (d, *J* = 1.5 Hz, 2H), 7.64 (dd, *J* = 1.5 Hz, *J* = 7.9 Hz, 2H), 7.40 (d, *J* = 7.9 Hz, 2H), 2.07 ppm (m, 8H); <sup>13</sup>C NMR (CDCl<sub>3</sub>, 75 MHz): δ = 156.1, 138.2, 136.0, 132.3, 121.5, 93.4, 57.8, 39.7, 27.1 ppm; HRMS (ESI/ASAP) calcd for C<sub>17</sub>H<sub>14</sub>I<sub>2</sub> [M<sup>+</sup>]: *m/z* 471.9185; found: 471.9192; m.p. 172 °C; *R*<sub>f</sub> = 0.6 (CH<sub>2</sub>Cl<sub>2</sub>/heptane; 1:9).

**2,7'-Bis(5-formyl-thiophen-2-yl)spiro[cyclopentane-1,9'-fluorene]**

**(2):** Air was removed from a solution of **B** (512 mg, 1.08 mmol), 5-formyl-2-thienylboronic acid (634 mg, 4.06 mmol), [PdCl<sub>2</sub>(dppf)] (14 mg, 0.02 mmol), and K<sub>2</sub>CO<sub>3</sub> (1460 mg, 10.56 mmol) in toluene/MeOH (30 mL, 2:1) by blowing argon for 30 min. Thereafter, the mixture was stirred at 75 °C for 20 h. The resulting mixture was poured into water (30 mL) and Et<sub>2</sub>O (30 mL). The organic layer was dried over Na<sub>2</sub>SO<sub>4</sub>, filtered through a short pad of silica (Et<sub>2</sub>O as eluent), and the solvent was evaporated. The resulting powder was recrystallized by slow cooling of a saturated solution in hot heptane to yield 449 mg (94%) of **2** as yellow crystals. <sup>1</sup>H NMR (CDCl<sub>3</sub>, 300 MHz): δ = 9.91 (s, 2H), 7.77 (d, *J* = 3.9 Hz, 2H), 7.76 (d, *J* = 7.9 Hz, 2H), 7.73 (d, *J* = 1.7 Hz, 2H), 7.69 (dd, *J* = 7.9 Hz, *J* = 1.7 Hz, 2H), 7.47 (d, *J* = 3.9 Hz, 2H), 2.20 (m, 8H); <sup>13</sup>C NMR (CDCl<sub>3</sub>, 75 MHz): δ = 182.7, 155.7, 154.7, 142.3, 140.0, 137.4, 132.8, 125.6, 124.0, 121.0, 50.0, 39.8, 27 ppm; FTIR (cm<sup>-1</sup>):  $\tilde{\nu}$  = 1650 (ν C=O); HRMS (ESI/ASAP) calcd for C<sub>27</sub>H<sub>21</sub>O<sub>2</sub>S<sub>2</sub> [M+H]<sup>+</sup>: *m/z* 441.0983; found: 441.0984; elemental analysis calcd (%) for C<sub>27</sub>H<sub>21</sub>O<sub>2</sub>S<sub>2</sub> (440.58 g mol<sup>-1</sup>): C 73.51, H 4.58; found: C 73.24, H 4.47; m.p. > 265 °C.

**2,7'-Bis(2-thienyl)spiro[cyclopentane-1,9'-fluorene]**

**(3):** A solution of 2-thienylmagnesium bromide in THF (0.3 M, 50.0 mL) was added dropwise to a mixture of **B** (1.55 g, 3.28 mmol) and [PdCl<sub>2</sub>(dppf)] (0.09 g, 0.11 mmol) and the reaction mixture was then heated to reflux for 48 h. After addition of ice, extraction with Et<sub>2</sub>O, drying over MgSO<sub>4</sub>, and filtering through a short pad of Celite, the solvent was evaporated. The crude compound was recrystallized by slow cooling of a saturated solution in hot heptane to yield 0.94 g (75%) of **3** as pale crystals. <sup>1</sup>H NMR (CDCl<sub>3</sub>, 300 MHz): δ = 7.68 (d, *J* = 7.9 Hz, 2H), 7.66 (d, *J* = 1.6 Hz, 2H), 7.60 (dd, *J* = 7.9 Hz, *J* = 1.6 Hz, 2H), 7.37 (dd, *J* = 3.6 Hz, *J* = 1.1 Hz, 2H), 7.30 (dd, *J* = 5.1 Hz, *J* = 1.1 Hz, 2H), 7.11 (dd, *J* = 5.1 Hz, *J* = 3.6 Hz, 2H), 2.19 ppm (m, 8H); <sup>13</sup>C NMR (CDCl<sub>3</sub>, 75 MHz): δ = 155.4, 145.2, 138.7, 133.9, 128.2, 125.1, 124.7, 123.1, 120.6, 120.1, 57.9, 40.0, 27.2 ppm; m.p. 196 °C.

**2,7'-Bis(5-iodo-thiophen-2-yl)spiro[cyclopentane-1,9'-fluorene]**

**(C):** *N*-Iodosuccinimide (369 mg, 1.64 mmol) was added to a solution of **3** (300 mg, 0.78 mmol) in CHCl<sub>3</sub>/AcOH<sub>gl</sub> (4 mL, 4:1). Then the solution was quickly warmed to 90 °C (the oil bath was heated at this temperature) for 5 min exactly. Then CHCl<sub>3</sub> was evaporated and the crude product was triturated in glacial acetic acid and filtered. The precipitate was washed with ethanol to give 506 mg (quantitative) of **C** as a yellow powder. <sup>1</sup>H NMR (CDCl<sub>3</sub>, 400 MHz): δ = 7.66 (dd, *J* = 7.9 Hz, *J* = 0.5 Hz, 2H), 7.55 (s, 2H), 7.50 (dd, *J* = 7.9 Hz, *J* = 1.6 Hz, 2H), 7.26 (d, *J* = 3.8 Hz, 2H), 7.02 (d, *J* = 3.8 Hz, 2H), 2.17 ppm (m, 8H); <sup>13</sup>C NMR (CDCl<sub>3</sub>, 100 MHz): δ = 155.5, 151.1, 139.0, 138.1, 133.2, 125.0, 124.6, 120.4, 120.3, 72.2, 57.9, 40.0, 27.2 ppm; HRMS (FD) calcd for C<sub>25</sub>H<sub>18</sub>I<sub>2</sub>S<sub>2</sub> [M<sup>+</sup>]: *m/z* 635.89393; found: 635.89411.

**2,7'-Bis(5-((1*E*)-2-[4-(*N,N*-dibutylamino)phenyl]ethenyl)thiophen-2-yl)spiro[cyclopentane-1,9'-fluorene]** **(4):** *t*BuOK (149 mg, 1.33 mmol) was added to a solution of **2** (149 mg, 0.34 mmol) and

4-(*N,N*-dibutylaminobenzyl)triphenylphosphonium iodide (413 mg, 0.68 mmol) in CH<sub>2</sub>Cl<sub>2</sub> (4 mL). The mixture was stirred at RT for 24 h. The resulting mixture was filtered through a short pad of Celite and the solvent evaporated. The crude product was purified by column chromatography (heptane/CH<sub>2</sub>Cl<sub>2</sub>, 2:1) to yield 202 mg (71%) of **4** as a yellow powder. <sup>1</sup>H NMR (CDCl<sub>3</sub>, 200 MHz): δ = 7.69 (d, *J* = 7.9 Hz, 2H), 7.66 (d, *J* = 1.7 Hz, 2H), 7.60 (dd, *J* = 7.9 Hz, *J* = 1.7 Hz, 2H), 7.28 (d, *J* = 3.8 Hz, 2H), 6.97 (d, *J* = 3.8 Hz, 2H), 6.87–7.00 (AB, *J*<sub>AB</sub> = 16.0 Hz, 4H), 6.62–7.32 (AA'XX', *J*<sub>AX</sub> = 8.9 Hz, 8H), 3.30 (dd, *J* = 7.9 Hz, *J* = 7.3 Hz, 8H), 2.20 (m, 8H), 1.57 (m, 8H), 1.38 (m, 8H), 0.96 ppm (t, *J* = 7.3 Hz, 12H); <sup>13</sup>C NMR (CDCl<sub>3</sub>, 75 MHz): δ = 155.4, 148.0, 143.7, 142.1, 138.5, 133.9, 128.9, 127.8, 125.8, 124.6, 124.2, 123.5, 120.0, 117.2, 111.8, 57.7, 50.9, 40.1, 29.6, 27.5, 20.5, 14.2 ppm; HRMS calcd for C<sub>57</sub>H<sub>66</sub>N<sub>2</sub>S<sub>2</sub> [M<sup>+</sup>]: *m/z* 842.4661; found: 842.4667; elemental analysis calcd (%) for C<sub>57</sub>H<sub>66</sub>N<sub>2</sub>S<sub>2</sub> (843.29 g mol<sup>-1</sup>): C 81.19, H 7.89, N 3.32, S 7.60; found: C 81.11, H 7.83, N 3.32, S 7.57; m.p. 181 °C; *R*<sub>f</sub> = 0.6 (heptane/CH<sub>2</sub>Cl<sub>2</sub>, 2:1).

**2,7,12-Tris(diphenylamino)-5,5',10,10',15,15'-hexabutyltruxene**

**(5):** A mixture of 2,7,12 triiodo-5,5',10,10',15,15'-hexabutyltruxene (2.86 g, 2.70 mmol), diphenylamine (2.4 g, 14.18 mmol), potassium carbonate (5.60 g, 40.50 mmol), copper powder (0.10 g, 1.56 mmol), and 18-crown-6 (0.04 g, 0.15 mmol) in *o*-dichlorobenzene (25 mL) under Ar was heated to reflux for 60 h. After cooling, the reaction mixture was diluted with CH<sub>2</sub>Cl<sub>2</sub> (100 mL) and filtered through a Celite pad. The solvents were evaporated to dryness and the residue was dissolved in petroleum ether for flash chromatography. The suspension was poured on a small silica pad (10 cm) and rinsed with petroleum ether to remove remaining *o*-dichlorobenzene. Then the column was eluted with CH<sub>2</sub>Cl<sub>2</sub> and the solvent was evaporated. To remove unconverted diphenylamine (same *R*<sub>f</sub> as compound **5**) the solid was recrystallized from heptane/ethyl acetate (1:1, 100 mL). Compound **5** was obtained as an off-white powder (2.56 g, 77%). <sup>1</sup>H NMR (CDCl<sub>3</sub>, 300 MHz): δ = 8.35 (d, *J* = 8.7 Hz, 3H), 7.31 (m, 12H), 7.21 (m, 15H), 7.05 (m, 9H), 2.81 (m, 6H), 1.89 (m, 6H), 0.96 (m, 12H), 0.62 (m, 12H), 0.57 ppm (t, *J* = 7.2 Hz, 18H); <sup>13</sup>C NMR (CDCl<sub>3</sub>, 75 MHz): δ = 155.0, 147.9, 146.0, 143.3, 137.9, 135.3, 129.2, 125.3, 124.1, 122.5, 121.9, 117.7, 55.3, 36.3, 26.6, 22.9, 14.0; HRMS calcd for C<sub>87</sub>H<sub>93</sub>N<sub>3</sub> [M<sup>+</sup>]: *m/z* 1179.73695; found: 1179.73884; elemental analysis calcd (%) for C<sub>87</sub>H<sub>93</sub>N<sub>3</sub> (1180.72 g mol<sup>-1</sup>): C 88.50, H 7.94, N 3.56; found: C 88.31, H 8.07, N 3.39; m.p. 263 °C.

**Photophysical characterization**

All photophysical properties were analyzed with freshly prepared air-equilibrated solutions at room temperature (293 K). UV/Vis absorption spectra were recorded with a Jasco V-570 spectrophotometer. Steady-state fluorescence measurements were performed on dilute solutions (optical density < 0.1) contained in standard 1 cm quartz cuvettes by using a Horiba (FluoroLog or FluoroMax) spectrometer in photon-counting mode. Fully corrected emission spectra were obtained for each compound at  $\lambda_{\text{ex}} = \lambda_{\text{max}}^{\text{Abs}}$  with an optical density at  $\lambda_{\text{ex}}$  of ≤ 0.1 to minimize internal absorption. Fluorescence quantum yields were measured according to literature procedures<sup>[46]</sup> by using fluorescein in 0.1 M NaOH ( $\Phi_{\text{F}} = 0.9$ ), quinine bisulfate in 0.5 M H<sub>2</sub>SO<sub>4</sub> ( $\Phi_{\text{F}} = 0.54$ ), or cresyl violet in MeOH ( $\Phi_{\text{F}} = 0.54$ ).

The molar decadic absorption coefficients of FONs [**1**] and [**4**] in water were calculated from the FONs concentrations derived from the total dye concentrations in water and the average number of dye subunits per FON (*N* = 29000 for **1** and *N* = 29700 for **4**). The average number of dye subunits per FONs *N* was estimated from the volume of the FONs (based on the FON diameter determined

by TEM) and the density relative to water (1.0). The global concentration of the dye in the FONs suspension was determined by taking an aliquot of the suspension, which was further lyophilized then dissolved in the same volume of THF. The concentration was then derived from the absorbance and the value of the molar extinction coefficient in THF ( $\epsilon^{\max} = 90\,000\text{ M}^{-1}\text{ cm}^{-1}$  for **1** and  $\epsilon^{\max} = 126\,000\text{ M}^{-1}\text{ cm}^{-1}$  for **4**) by using the Beer–Lambert law.

### Preparation of FONs [1] and [4]

The nanoparticles were prepared by the nanoprecipitation method, which consisted of instantaneous addition of a solution of **1** or **4** in THF (1 mM) in distilled water under sonication at 10 W for 3 min (VibraCell 1300 W sonicator probe with 6 mm diameter). The total amount of THF in water was set to be lower than 1%. Quickly after the addition, the solution evolved from colorless to yellow.

### Characterization of FONs [1] and [4]

TEM imaging was carried out with a Hitachi H7650. Copper grids coated with a carbon membrane were pretreated by using the glow-discharge technique to yield to positively charged grids and thus help the interaction between the FONs and the grid. One droplet of aqueous FONs suspension was deposited on the grid followed, once the excess of liquid was drawn off with paper, by a staining procedure with uranyl acetate. DLS experiments were performed with a Horiba SZ-100Z instrument operating at 173°. Hydrodynamic diameters  $d_h$  were calculated from diffusion coefficients by using the Stokes–Einstein equation. All correlogram analyses were performed with the software supplied by the manufacturer and are represented in scattering light intensity. Zeta-potential analysis was performed with the Horiba SZ-100Z instrument. Several measurements were performed for each sample according to a predefined operating procedure.

### Electrochemical characterization

Cyclic voltammetry was performed with a PGSTAT30 Autolab potentiostat connected to a conventional three-electrode cell with a silver-wire quasireference electrode, a platinum-wire counter electrode, and a platinum working electrode. Potential calibration of the silver wire was performed with a standard  $\text{Fc}/\text{Fc}^+$  redox couple (taken as 0.342 V vs.  $\text{SCE}^{(47)}$ ) after the measurements. For the study of FONs [1], a glassy carbon (GC) electrode and a Ag/AgCl electrode were used as working electrode and reference electrode, respectively, but the potential was referred to SCE. Prior to measurement, both Pt disk and GC electrode were polished with alumina slurries of different particle sizes, rinsed thoroughly with Milli-Q water between each polishing step, and sonicated in water and ethanol, respectively, followed by a final rinse with acetone and drying with  $\text{N}_2$  stream.

Spectroelectrochemical spectra were recorded with a Cary 100 UV/Vis spectrophotometer and Cary Eclipse spectrophotometer with a  $\mu$ -Autolab type III potentiostat. The spectroelectrochemical cell was constructed by loading a transparent Pt mesh working electrode into a thin-layer channel with 1 mm path length in the quartz cuvette and mounting the other two electrodes above the channel.

ECL intensity was measured with a Hamamatsu R5070 photomultiplier tube with a Hamamatsu C9525 high-voltage power supply. The PMT detector was held at  $-750\text{ V}$  and placed a few millimeters in front of the working electrode. The output signal was amplified by a Keithley 6485 Picoammeter before acquisition via the second input channel of the PGSTAT30 AUTOLAB potentiostat. ECL spectra

were recorded with a Princeton Instruments Acton SpectraPro 2300i after the CCD camera, cooled to  $-115\text{ }^\circ\text{C}$  with liquid  $\text{N}_2$ . The electrochemical cell was built with a glass slide on the bottom in order to record the ECL signal. The optical fiber connected to the device is placed close to this glass slide in front of the working electrode.

### Acknowledgements

H.L. acknowledges the China Scholarship Council for his PhD fellowship. M.B.-D. acknowledges financial support from the Conseil Régional d'Aquitaine (Chair of Excellence to M.B.-D. and fellowship to J.D.). **This study was achieved within the context of the Laboratory of Excellence TRAIL ANR-10-LABX-57.** TEM microscopy was done in the Bordeaux Imaging Center (UMS 3420 CNRS - University of Bordeaux/Inserm US4). The help of Sabrina Lacomme is acknowledged.

**Keywords:** dyes/pigments • electrochemistry • luminescence • nanoparticles • spiro compounds

- [1] a) A. Kanitz, J. Schumann, M. Scheffel, S. Rajoelson, W. Rogler, H. Hartmann, D. Rohde, *Chem. Lett.* **2002**, 896–897; b) D. M. Welsh, A. Kumar, E. W. Meijer, J. R. Reynolds, *Adv. Mater.* **1999**, *11*, 1379–1382; c) A. Kumar, D. M. Welsh, M. C. Morvant, F. Piroux, K. A. Abboud, J. R. Reynolds, *Chem. Mater.* **1998**, *10*, 896–902.
- [2] a) L. M. Goldenberg, M. R. Bryce, M. C. Petty, *J. Mater. Chem.* **1999**, *9*, 1957–1974; b) T. M. Swager, *Acc. Chem. Res.* **1998**, *31*, 201–207.
- [3] H. Röckel, J. Huber, R. Gleiter, W. Schuhmann, *Adv. Mater.* **1994**, *6*, 568–571.
- [4] a) G. Barbarella, L. Favaretto, G. Sotgiu, M. Zambianchi, V. Fattori, M. Cocchi, F. Cacialli, G. Gigli, R. Cingolani, *Adv. Mater.* **1999**, *11*, 1375–1379; b) A. Cazzato, M. L. Capobianco, M. Zambianchi, L. Favaretto, C. Bettini, G. Barbarella, *Bioconjugate Chem.* **2007**, *18*, 318–322; c) A. B. Nepomnyashchii, R. J. Ono, D. M. Lyons, C. W. Bielawski, J. L. Sessler, A. J. Bard, *Chem. Sci.* **2012**, *3*, 2628–2638; d) M. L. Capobianco, G. Barbarella, A. Manetto, *Molecules* **2012**, *17*, 910.
- [5] I. F. Perepichka, D. F. Perepichka, *Handbook of thiophene-based materials: applications in organic electronics and photonics*, Wiley, Hoboken, **2009**.
- [6] F. Diederich, P. J. Stang, *Metal-catalyzed cross-coupling reactions*, John Wiley, Hoboken, **2008**.
- [7] a) P. Bäuerle, *Adv. Mater.* **1992**, *4*, 102–107; b) P. Rapta, K. Haubner, P. Machata, V. Lukeš, M. Rosenkranz, S. Schiemenz, S. Klod, H. Kivelä, C. Kvarnström, H. Hartmann, *Electrochim. Acta* **2013**, *110*, 670–680; c) U. Mitschke, P. Bäuerle, *J. Chem. Soc. Perkin Trans. 1* **2001**, 740–753.
- [8] D. Rohde, L. Dunsch, A. Tabet, H. Hartmann, J. Fabian, *J. Phys. Chem. B* **2006**, *110*, 8223–8231.
- [9] a) D. Fichou, *J. Mater. Chem.* **2000**, *10*, 571–588; b) U. Mitschke, P. Bäuerle, *J. Mater. Chem.* **2000**, *10*, 1471–1507; c) I. F. Perepichka, D. F. Perepichka, H. Meng, F. Wudl, *Adv. Mater.* **2005**, *17*, 2281–2306.
- [10] a) F. Garnier, R. Hajlaoui, A. Yassar, P. Srivastava, *Science* **1994**, *265*, 1684–1686; b) B. S. Ong, Y. Wu, P. Liu, S. Gardner, *J. Am. Chem. Soc.* **2004**, *126*, 3378–3379.
- [11] N. Sariciftci, L. Smilowitz, A. J. Heeger, F. Wudl, *Science* **1992**, *258*, 1474–1476.
- [12] V. Getautis, A. Stanisaukaite, O. Paliulis, S. Uss, V. Uss, *J. Prakt. Chem.* **2000**, *342*, 58–62.
- [13] a) K. M. Omer, S.-Y. Ku, J.-Z. Cheng, S.-H. Chou, K.-T. Wong, A. J. Bard, *J. Am. Chem. Soc.* **2011**, *133*, 5492–5499; b) M. I. Mangione, R. A. Spanevello, A. Rumbero, D. Heredia, G. Marzari, L. Fernandez, L. Otero, F. Fungo, *Macromolecules* **2013**, *46*, 4754–4763.
- [14] A. J. Bard, *Electrogenerated chemiluminescence*, CRC Press, Marcel Dekker, New York, **2004**.

- [15] a) W. Miao, *Chem. Rev.* **2008**, *108*, 2506–2553; b) M. M. Richter, *Chem. Rev.* **2004**, *104*, 3003–3036; c) L. Hu, G. Xu, *Chem. Soc. Rev.* **2010**, *39*, 3275–3304.
- [16] W. Miao, J.-P. Choi, A. J. Bard, *J. Am. Chem. Soc.* **2002**, *124*, 14478–14485.
- [17] M.-M. Chang, T. Saji, A. J. Bard, *J. Am. Chem. Soc.* **1977**, *99*, 5399–5403.
- [18] J.-P. Choi, K.-T. Wong, Y.-M. Chen, J.-K. Yu, P.-T. Chou, A. J. Bard, *J. Phys. Chem. B* **2003**, *107*, 14407–14413.
- [19] Z. Liu, W. Qi, G. Xu, *Chem. Soc. Rev.* **2015**, *44*, 3117–3142.
- [20] a) H. Yang, J. K. Leland, D. Yost, R. J. Massey, *Nat. Biotechnol.* **1994**, *12*, 193–194; b) F. Deiss, C. N. LaFratta, M. Symer, T. M. Blicharz, N. Sojic, D. R. Walt, *J. Am. Chem. Soc.* **2009**, *131*, 6088–6089.
- [21] a) G. J. Barbante, E. H. Doeven, E. Kerr, T. U. Connell, P. S. Donnelly, J. M. White, T. López, S. Laird, D. J. D. Wilson, P. J. Barnard, C. F. Hogan, P. S. Francis, *Chem. Eur. J.* **2014**, *20*, 3322–3332; b) K. N. Swanick, S. Ladouceur, E. Zysman-Colman, Z. Ding, *Chem. Commun.* **2012**, *48*, 3179–3181; c) M. Schmittel, H.-W. Lin, *Angew. Chem. Int. Ed.* **2007**, *46*, 893–896; *Angew. Chem.* **2007**, *119*, 911–914.
- [22] a) S. Zanarini, E. Rampazzo, S. Bonacchi, R. Juris, M. Marcaccio, M. Montalti, F. Paolucci, L. Prodi, *J. Am. Chem. Soc.* **2009**, *131*, 14208; b) S. Zanarini, M. Felici, G. Valenti, M. Marcaccio, L. Prodi, S. Bonacchi, P. Contreas-Carballada, R. M. Williams, M. C. Feiters, R. J. M. Nolte, L. De Cola, F. Paolucci, *Chem. Eur. J.* **2011**, *17*, 4640–4647; c) G. Valenti, E. Rampazzo, S. Bonacchi, T. Khajvand, R. Juris, M. Montalti, M. Marcaccio, F. Paolucci, L. Prodi, *Chem. Commun.* **2012**, *48*, 4187–4189; d) E. Rampazzo, S. Bonacchi, D. Genovese, R. Juris, M. Marcaccio, M. Montalti, F. Paolucci, M. Sgarzi, G. Valenti, N. Zaccheroni, L. Prodi, *Coord. Chem. Rev.* **2012**, *256*, 1664–1681; e) H. Lin, M. E. Cinar, M. Schmittel, *Dalton Trans.* **2010**, *39*, 5130–5138; f) M. Schmittel, Q. Shu, M. E. Cinar, *Dalton Trans.* **2012**, *41*, 6064–6068; g) P. Natarajan, M. Schmittel, *J. Org. Chem.* **2013**, *78*, 10383–10394; h) E. H. Doeven, E. M. Zammit, G. J. Barbante, C. F. Hogan, N. W. Barnett, P. S. Francis, *Angew. Chem. Int. Ed.* **2012**, *51*, 4354–4357; *Angew. Chem.* **2012**, *124*, 4430–4433; i) E. H. Doeven, E. M. Zammit, G. J. Barbante, P. S. Francis, N. W. Barnett, C. F. Hogan, *Chem. Sci.* **2013**, *4*, 977–982; j) K. N. Swanick, S. Ladouceur, E. Zysman-Colman, Z. Ding, *Angew. Chem. Int. Ed.* **2012**, *51*, 11079–11082; *Angew. Chem.* **2012**, *124*, 11241–11244; k) Z. Ding, B. M. Quinn, S. K. Haram, L. E. Pell, B. A. Korgel, A. J. Bard, *Science* **2002**, *296*, 1293–1297; l) K. N. Swanick, M. Hesari, M. S. Workentin, Z. Ding, *J. Am. Chem. Soc.* **2012**, *134*, 15205–15208; m) N. Myung, Z. Ding, A. J. Bard, *Nano Lett.* **2002**, *2*, 1315–1319; n) J.-W. Oh, Y. O. Lee, T. H. Kim, K. C. Ko, J. Y. Lee, H. Kim, J. S. Kim, *Angew. Chem. Int. Ed.* **2009**, *48*, 2522–2524; *Angew. Chem.* **2009**, *121*, 2560–2562.
- [23] J. Daniel, A. G. Godin, M. Palayret, B. Lounis, L. Cognet, M. Blanchard-Desce, *J. Phys. D* **2016**, *49*, 084002.
- [24] K. M. Omer, S.-Y. Ku, Y.-C. Chen, K.-T. Wong, A. J. Bard, *J. Am. Chem. Soc.* **2010**, *132*, 10944–10952.
- [25] a) F. Fungo, K.-T. Wong, S.-Y. Ku, Y.-Y. Hung, A. J. Bard, *J. Phys. Chem. B* **2005**, *109*, 3984–3989; b) F. Polo, F. Rizzo, M. Veiga-Gutierrez, L. De Cola, S. Quici, *J. Am. Chem. Soc.* **2012**, *134*, 15402–15409.
- [26] S. Destri, M. Pasini, C. Botta, W. Porzio, F. Bertini, L. Marchio, *J. Mater. Chem.* **2002**, *12*, 924–933.
- [27] Y. Yuan, S. Han, L. Hu, S. Parveen, G. Xu, *Electrochim. Acta* **2012**, *82*, 484–492.
- [28] C. Hansch, A. Leo, R. W. Taft, *Chem. Rev.* **1991**, *91*, 165–195.
- [29] A. Diaz, J. Crowley, J. Bargon, G. Gardini, J. Torrance, *J. Electroanal. Chem.* **1981**, *121*, 355–361.
- [30] a) P. Audebert, F. Miomandre, *Chem. Sci.* **2013**, *4*, 575–584; b) C. Quinton, V. Alain-Rizzo, C. Dumas-Verdes, F. Miomandre, G. Clavier, P. Audebert, *RSC Adv.* **2014**, *4*, 34332–34342.
- [31] C. Katan, S. Tretiak, M. H. V. Werts, A. J. Bain, R. J. Marsh, N. Leonczek, N. Nicolaou, E. Badaeva, O. Mongin, M. Blanchard-Desce, *J. Phys. Chem. B* **2007**, *111*, 9468–9483.
- [32] a) Y.-H. Bi, Z.-L. Huang, B. Liu, Q.-J. Zou, J.-H. Yu, Y.-D. Zhao, Q.-M. Luo, *Electrochem. Commun.* **2006**, *8*, 595–599; b) I. Yilmaz, *New J. Chem.* **2008**, *32*, 37–46.
- [33] a) K. M. Omer, S.-Y. Ku, K.-T. Wong, A. J. Bard, *J. Am. Chem. Soc.* **2009**, *131*, 10733–10741; b) K. M. Omer, S.-Y. Ku, K.-T. Wong, A. J. Bard, *Angew. Chem. Int. Ed.* **2009**, *48*, 9300–9303; *Angew. Chem.* **2009**, *121*, 9464–9467.
- [34] F. Kanoufi, Y. Zu, A. J. Bard, *J. Phys. Chem. B* **2001**, *105*, 210–216.
- [35] B. D. Stringer, L. M. Quan, P. J. Barnard, D. J. D. Wilson, C. F. Hogan, *Organometallics* **2014**, *33*, 4860–4872.
- [36] a) A. Kapturkiewicz, Z. R. Grabowski, J. Jasny, *J. Electroanal. Chem.* **1990**, *279*, 55–65; b) A. Kapturkiewicz, *Chem. Phys.* **1992**, *166*, 259–273.
- [37] a) M. Shen, X.-H. Zhu, A. J. Bard, *J. Am. Chem. Soc.* **2013**, *135*, 8868–8873; b) C. Adam, A. Wallabregue, H. Li, J. Gouin, R. Vanel, S. Grass, J. Bosson, L. Bouffier, J. Lacour, N. Sojic, *Chem. Eur. J.* **2015**, *21*, 19243–19249; c) A. B. Nepomnyashchii, M. Bröring, J. Ahrens, A. J. Bard, *J. Am. Chem. Soc.* **2011**, *133*, 8633–8645.
- [38] a) Y.-L. Chang, R. E. Palacios, F.-R. F. Fan, A. J. Bard, P. F. Paul, F. Barbara, *J. Am. Chem. Soc.* **2008**, *130*, 8906–8907; b) J. Suk, Z. Wu, L. Wang, A. J. Bard, *J. Am. Chem. Soc.* **2011**, *133*, 14675–14685.
- [39] a) Z. Guo, Y. Shen, M. Wang, F. Zhao, S. Dong, *Anal. Chem.* **2004**, *76*, 184–191; b) S. Deng, H. Ju, *Analyst* **2013**, *138*, 43–61; c) M.-J. Li, Z. Chen, V. W.-W. Yam, Y. Zu, *ACS Nano* **2008**, *2*, 905–912; d) F. Pinaud, L. Russo, S. Pinet, I. Gosse, V. Ravaine, N. Sojic, *J. Am. Chem. Soc.* **2013**, *135*, 5517–5520.
- [40] H. Masuhara, H. Nakanishi and K. Sasaki, *Single Organic Nanoparticles*, Springer, Berlin, **2003**.
- [41] S. Bonacchi, D. Genovese, R. Juris, M. Montalti, L. Prodi, E. Rampazzo, N. Zaccheroni, *Angew. Chem. Int. Ed.* **2011**, *50*, 4056–4066; *Angew. Chem.* **2011**, *123*, 4142–4152.
- [42] M. Hesari, K. N. Swanick, J.-S. Lu, R. Whyte, S. Wang, Z. Ding, *J. Am. Chem. Soc.* **2015**, *137*, 11266–11269.
- [43] M. Hesari, M. S. Workentin, Z. Ding, *Chem. Eur. J.* **2014**, *20*, 15116–15121.
- [44] R. C. Bansal, E. J. Eisenbraun, R. J. Ryba, *Org. Prep. Proced. Int.* **1987**, *19*, 258–260.
- [45] S.-C. Yuan, H.-B. Chen, Y. Zhang, J. Pei, *Org. Lett.* **2006**, *8*, 5701–5704.
- [46] a) D. F. Eaton, *Pure Appl. Chem.* **1988**, *60*, 1107–1114; b) G. A. Crosby, J. N. Demas, *J. Phys. Chem.* **1971**, *75*, 991–1024.
- [47] V. V. Pavlishchuk, A. W. Addison, *Inorg. Chim. Acta* **2000**, *298*, 97–102.

Received: January 28, 2016

Published online on July 11, 2016